

# A Tunable Single-Molecule Light-Emitting Diode with Single-Photon Precision

Chen Yang, Yilin Guo, Shuyao Zhou, Zhirong Liu, Zitong Liu,\* Deqing Zhang, and Xuefeng Guo\*

**A robust single-molecule light-emitting diode (SM-LED) with high color purity, linear polarization, and efficiency tunability is prepared by covalently integrating one fluorescent molecule into nanogapped graphene electrodes. Furthermore, single-molecule Förster resonance energy transfer from the electroluminescent center to different accepters is achieved through rational molecular engineering, enabling construction of a multicolor SM-LED. All these characterizations are accomplished in the photoelectrical integration system with high temporal/spatial/energy resolution, demonstrating the capability of the single-photon emission of SM-LEDs. The success in developing high-performance SM-LEDs inspires the development of the next generation of commercial display devices and promises a single-photon emitter for use in quantum computation and quantum communication.**

## 1. Introduction

Nowadays, society's demand<sup>[1–5]</sup> for light relates not only to illumination. Applications of light in terms of display,<sup>[6]</sup> operation,<sup>[7]</sup> and energy<sup>[8]</sup> are gaining wide interest, especially in the

example of display devices used in daily life. As the newest generation of light-emitting diodes (LEDs) used in devices, quantum-dot light-emitting diodes (QD-LEDs) have a full range of pure color (i.e., color tunable by size, a full width at half maximum (FWHM) of approximately tens of nanometers),<sup>[9]</sup> high integration with a high definition screen and virtual/augmented reality,<sup>[4]</sup> and high quantum efficiency and bright emission,<sup>[9]</sup> and they thus have good application potential. Naturally, the molecule being the basic quantum system inspires the concept of constructing a LED using only one molecule, i.e., a single-molecule light-emitting diode (SM-LED) featuring higher atomic

economy and integration, tunable color purity through precise organic synthesis, controllable energy band alignment, and the avoidance of intermolecular fluorescence quenching.<sup>[9]</sup> In fact, the physical world we see is built by molecules. Therefore, using a single molecule as a display pixel can most intrinsically represent the real world, which is the ultimate goal of display devices.

However, device engineering at the molecular level has always been a nontrivial task. A typical example of such engineering is the miniaturization of silicon-based microelectronic devices and the continuation of Moore's law.<sup>[10]</sup> To this end, the preparation of a multifunctional molecular device via a bottom-up pathway is a promising strategy.<sup>[11,12]</sup> Motivated by the initial theoretical proposal of a rectifier comprising individual D- $\sigma$ -A molecules,<sup>[13]</sup> various functional single-molecule devices such as the field-effect transistor,<sup>[14,15]</sup> rectifier,<sup>[16,17]</sup> switch,<sup>[18,19]</sup> and memristor<sup>[20]</sup> have been realized and continuously improved through long-term optimization of functional molecular centers, electrode materials, and the interface coupling.<sup>[11,12,21]</sup>


To realize a microscopic,<sup>[22]</sup> especially molecular-scale, light-emitting device, several huge challenges in the preparation and characterization must be overcome for efficient display and operation. First, emission in the visible-light region (380–880 nm) generally requires a working bias voltage ( $V_w$ ) of at least 1.4 V (excluding the upconversion mechanism) and thus necessitates the robustness of the molecular device (in particular the contact interface between the molecule and electrodes). Second, high quantum efficiency requires alignment of the energy band between the electroluminescent center and electrodes, and the avoidance of nonradiative loss. Finally, the characterization of the emission from one molecule requires the resolution on time, spatial, and energy scales.

C. Yang, Y. Guo, S. Zhou, Z. Liu, X. Guo  
 Beijing National Laboratory for Molecular Sciences  
 National Biomedical Imaging Center  
 College of Chemistry and Molecular Engineering  
 Peking University  
 292 Chengfu Road, Haidian District, Beijing 100871, P. R. China  
 E-mail: guoxf@pku.edu.cn

Z. Liu  
 State Key Laboratory of Applied Organic Chemistry  
 College of Chemistry and Chemical Engineering  
 Lanzhou University  
 Lanzhou, Gansu 730000, P. R. China  
 E-mail: liuzt@lzu.edu.cn

D. Zhang  
 Beijing National Laboratory for Molecular Sciences  
 CAS Key Laboratory of Organic Solids  
 Institute of Chemistry  
 Chinese Academy of Sciences  
 Beijing 100190, P. R. China

X. Guo  
 Center of Single-Molecule Sciences  
 Institute of Modern Optics  
 Frontiers Science Center for New Organic Matter  
 College of Electronic Information and Optical Engineering  
 Nankai University  
 38 Tongyan Road, Jinnan District, Tianjin 300350, P. R. China

 The ORCID identification number(s) for the author(s) of this article can be found under <https://doi.org/10.1002/adma.202209750>.

DOI: 10.1002/adma.202209750

Since the first report of single-molecule electroluminescence (SM-EL),<sup>[23,24]</sup> the innovation of the preparation technology,<sup>[25–28]</sup> as well as the control of the emission characteristics including color<sup>[29,30]</sup> and linewidth,<sup>[31]</sup> have been achieved by unremitting efforts. To further optimize the stability and performance, here the requirements of a robust molecule–electrode contact interface and the energy band alignment were addressed by covalent anchoring on graphene electrodes and gate regulation by the back gate, respectively. The triangular configuration of graphene with atomic-scale terminals also affords the ability of forming point contacts and thus the intermediate decoupling between the luminous center and electrodes. In addition, diverse functions of this SM-LED with high linear polarization and narrow color distribution, as well as the tunability of efficiency, photon number, and color toward practical applications, were reported.

## 2. Fabrication and Characterization of SM-LEDs

Using a covalent bond is the ideal strategy for reliably connecting electroluminescent molecules and electrodes to tolerate a high working voltage. Herein, we introduce the stable amide bond as the interface to realize charge transmission and decoupling. A carbazole-derived molecular bridge, the most challenging blue-light-emission group ( $V_w > 2.5$  V), was designed and integrated into nanogapped graphene electrodes via a solution process<sup>[32]</sup> (Figure 1a), which enables low-cost industrial production comparable to that of QD-LEDs. In particular, a functional side chain was designed to regulate the emission wavelength via further modification (see below). The detailed molecular synthetic route and device fabrication are provided in Scheme S1 and Figures S1 and S2, Supporting Information. The successful connection can be characterized by  $I$ – $V$  curves

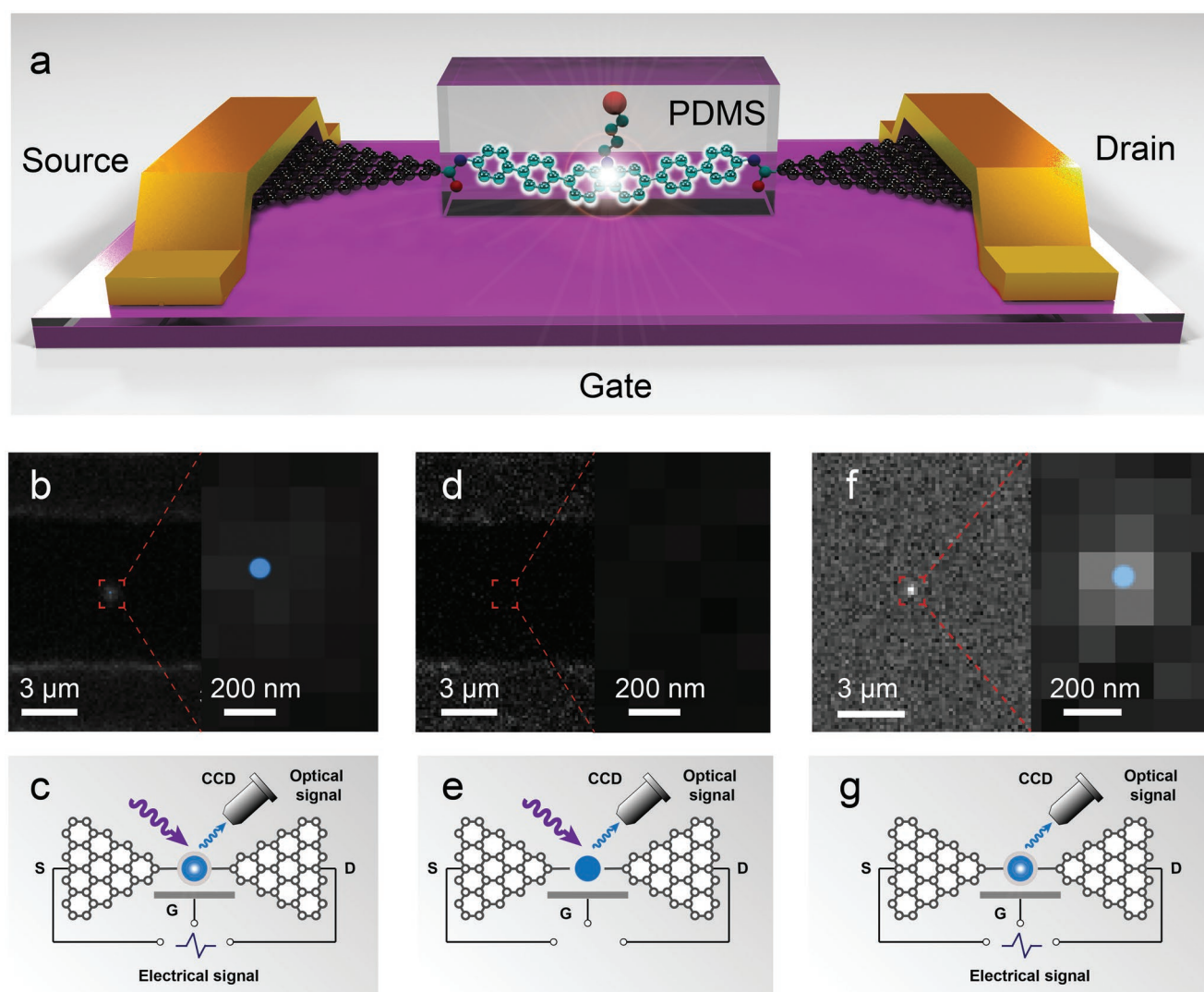


**Figure 1.** Schematic illustration and imaging of an SM-LED. a) Schematic representation of the device. The EL molecular center was covalently integrated into graphene point electrodes and encapsulated by PDMS. Au electrodes were introduced for application of the bias voltage and the Si wafer for application of the gate voltage. b) Superhigh-resolution image of an SM-LED by STORM and c) the corresponding experimental setup. Light: 365 nm;  $V_d = 4$  V;  $V_g = 8$  V. d) Superhigh-resolution image of the same SM-LED without the electric input, showing no obvious light spot, and e) the corresponding experimental setup. Light: 365 nm. f) Superhigh-resolution image of the same SM-LED without excited light and g) the corresponding experimental setup.  $V_d = 4$  V;  $V_g = 8$  V.

before (no response) and after (recovered to some extent) the molecular connection (Figures S3 and S4, Supporting Information). Under optimized conditions, the connection yield reached  $\approx 22\%$  for  $\approx 12$  of the 55 devices on the same silicon chip (Figure S3, Supporting Information), which demonstrates the reproducibility and reliability of the design. The statistical analysis presented in the Supporting Information demonstrates that the  $I$ - $V$  curve has  $\approx 90\%$  probability of originating from only one molecular connection between the electrodes (see the Supporting Information). More convincingly, a super-resolution fluorescence microscope was integrated into a single-molecule electrical monitoring platform (Figure S5, Supporting Information) to characterize the molecular connection and photon-emission behavior (see below). To avoid the electric burning of the molecular nanocircuit, the single-molecule junction was encapsulated by a polydimethylsiloxane (PDMS) with high light transmittance at room temperature, which will be crucial for broad practical applications in the future, rather than making measurements in a vacuum (or applying cryogenics)<sup>[24,25]</sup> (Figure 1a). Approximately 15 h lifetime (Figure S6, Supporting Information) of the luminescent SM-LED with electric inputs demonstrates its high stability experimentally.

Gold electrodes were used to connect the external circuit with the single-molecule junction. A heavily doped Si wafer with  $\approx 300$  nm  $\text{SiO}_2$  as the gate electrode regulated the molecular energy level<sup>[33]</sup> (Figure 1a). With electric inputs (Figure 1b,c, source-drain voltage ( $V_d$ ) = 4 V, gate voltage ( $V_g$ ) = 8 V), the site of the molecular connection was located through stochastic optical reconstruction microscopy (STORM).<sup>[34]</sup> The super-resolution image shows only one bright point ( $<200$  nm, the diffraction limit), again strongly showing the single-molecule connection. To further distinguish whether this optical signal originates from photoluminescence (PL) or electroluminescence (EL), characterizations were conducted without electric inputs (Figure 1d,e) or excited light (Figure 1f,g). As shown in Figure 1f, the optical signal (the EL) from the single-molecule site has a close relation with the electric input, whereas the PL has low efficiency (Figure 1d), implying a strong nonradiative process.<sup>[35,36]</sup> This observation is most likely owing to the different scenarios of the energy level alignment between molecule and electrodes in presence or absence of the bias voltage. To minimize the background noise, no excited light was adopted in the further optical characterization of the SM-EL.

The synchronous trigger of the optical and electrical systems was well designed and achieved (Figure S5, Supporting Information). With the application of periodic square waves of  $V_d$  and  $V_g$  (Figure 2a,e), the optical and electrical signals were recorded synchronously. Accompanied by the abrupt change of the source-drain current ( $I_d$ ) (Figure 2b,f), the SM-LED turned on at higher-level electric inputs (Figure 2c,g), which indicates the requirement of the energy to form excited states (see below). Note that the SM-EL was not continuous, implying a quantized emission behavior, which can be distinguished as “bright” and “dark” states on the measured time scale (Figure 2c,d,g,h, insets). In addition, the synchronously recorded electrical signal shows fluctuations (with low and high conductances) (Figure 2b,f), which are faithful to the optical signal in the “bright” and “dark” stages (Figure 2d,h, insets, also see Videos S1 and S2 in the Supporting Information). The

corresponding 2D statistical results indicate strong anticorrelation between these two signals (Figure 2d,h), implying that two electron transmission modes correspond to the “bright” and “dark” states, respectively. Herein, we propose that only the highest occupied molecular orbital (HOMO) (path ①) or HOMO + lowest unoccupied molecular orbital (LUMO) (path ②) dominates electron transmission in accounting for the dark and bright states, respectively (Figure 3b). In the latter case, the consumption of extra energy for an electron jumping to the molecular LUMO from the left electrode and another electron jumping simultaneously to the right electrode from the molecular HOMO decreases the current and produces the excited state. The relaxation of the excited state back to the ground state then leads to the SM-EL. The orthogonal regulation of the molecular orbit versus the electrode's Fermi level and theoretical studies (see below) further support this mechanism (Figures S7–S16, Supporting Information). It is seen that the combined photoelectrical characterization of the single molecule provides a new insight to the inherent (photo)physical properties.

### 3. Energy Level Analysis and Efficiency Regulation

The alignment of the energy band between the frontier molecular orbitals and the Fermi level of the electrodes is crucial for different kinds of optoelectronic device,<sup>[37,38]</sup> including SM-LEDs. Theoretical analysis of the molecular orbitals (i.e., the energy band) for electron transmission is presented in Figure 3a (0–2 V) and Figure S17 (Supporting Information) (2–8 V). The HOMO ( $\approx -0.29$  eV) was determined as the dominant transmission channel at  $V_g = 0$  V (close to the Fermi level, whereas the LUMO was at  $\approx 2.46$  eV, the corresponding eigenstates were provided in Figure S18 in the Supporting Information). With the addition of the positive  $V_g$  on the Si substrate (0–8 V set in the theoretical analysis), the transmission spectra shift downward as a whole in energy relative to the graphene Fermi level (set at zero) (Figure 3a,b and Figure S17 (Supporting Information)). According to the SM-EL mechanism proposed above, the electron transmission from the left electrode to the molecular LUMO should be regarded as the determining factor owing to the mismatch of the energy level (e.g., the energy barrier was  $\approx 1.46$  eV at  $V_d = 2$  V and  $V_g = 0$  V). The observed SM-EL (very little) can be attributed to the thermal fluctuation of the electron energy, where the possibility ( $P$ ) can be fitted by the Boltzmann distribution ( $P = \exp(-E_a/k_B T)$ ). The theoretical  $P$  of the SM-EL as a function of  $V_d$  and  $V_g$  is presented in Figure 3c. With increasing electric inputs,  $P$  increases exponentially until alignment of the energy band at  $P = 1$ . The effective upconversion SM-EL at low electric input is worthy of clarification in the future to meet the need for energy sustainability as in the cases of phonon- or plasma-assisted ELs.<sup>[39]</sup> The experimental efficiency of the SM-EL is presented in Figure 3d–f, which shows the precise tunability by electric inputs. The occupancy of the bright state versus  $V_d$  and  $V_g$  was derived using the recorded optical and electrical signals (Figure 3d, also see Video S3 in the Supporting Information). The consistent variations have a similar trend with the theoretical results (Figure 3c). Note that the experimental  $V_g$  is higher owing to the weak molecule–gate coupling for the back gate.<sup>[14]</sup> Furthermore, the number of emitted

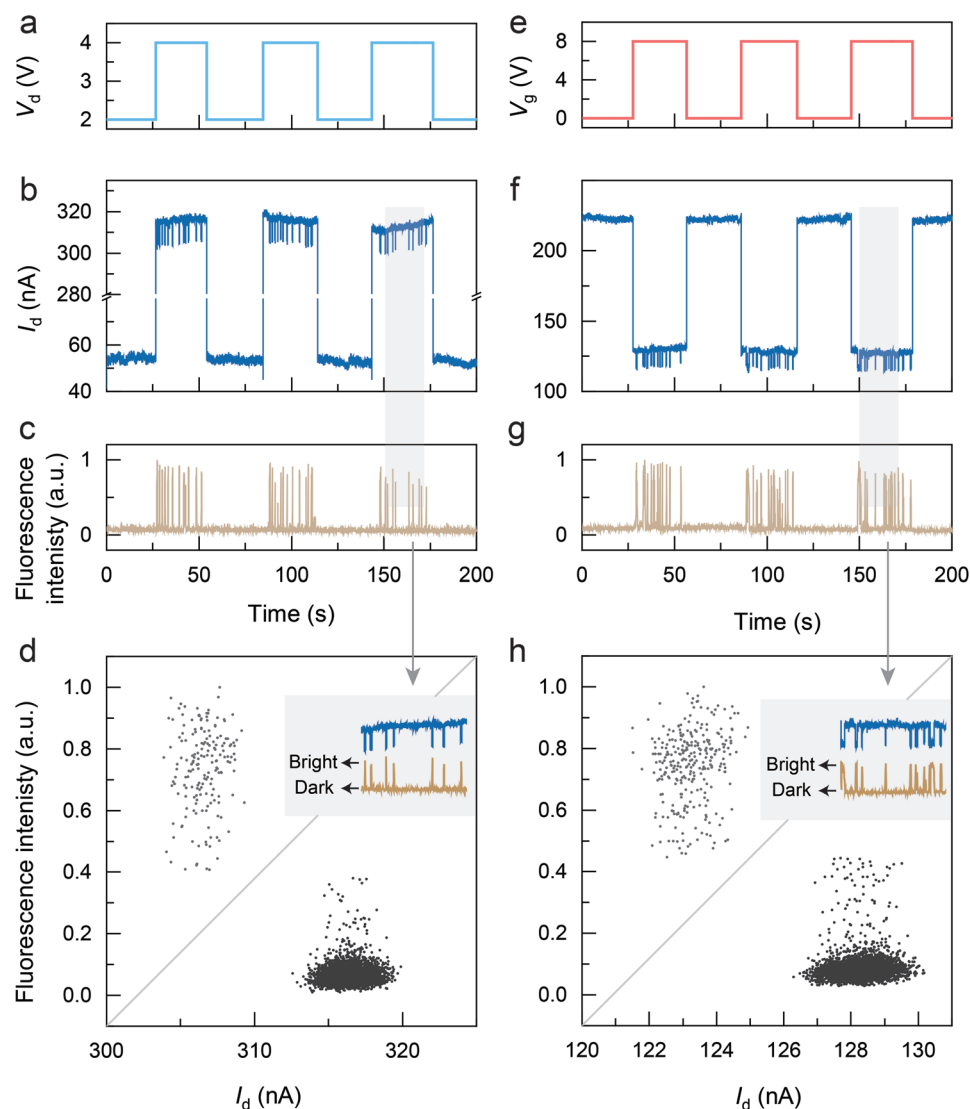


**Figure 2.** Characterization of an SM-LED by photoelectric integration. a) Square-wave  $V_d$  input (2/4 V) with a constant  $V_g$  of 6 V. b) The corresponding electrical signal  $I_d$  at square-wave  $V_d$  (2/4 V) and constant  $V_g$  (6 V). c) Simultaneous recorded fluorescence intensity (normalized) at the single-molecule site at square-wave  $V_d$  (2/4 V) and constant  $V_g$  (6 V). d) 2D mapping of the optical and electrical signals at square-wave  $V_d$  (2/4 V) and constant  $V_g$  (6 V). The insets show magnified views of the regions marked in (b) and (c). e) Square-wave  $V_g$  input (0/8 V) with a constant  $V_d$  of 3 V. f) The corresponding electrical signal  $I_d$  at square-wave  $V_g$  (0/8 V) and constant  $V_d$  (3 V). g) Simultaneous recorded fluorescence intensity (normalized) at the single-molecule site at square-wave  $V_g$  (0/8 V) and constant  $V_d$  (3 V). h) 2D mapping of the optical and electrical signals at square-wave  $V_g$  (0/8 V) and constant  $V_d$  (3 V). Insets are magnified views of the regions marked in (f) and (g).

photons versus  $V_d$  and  $V_g$  increases exponentially, which is consistent with theory (Figure 3c), before reaching a plateau, which indicates the maximum work ability of the SM-LED in the situation of well alignment of the energy band (Figure 3b).

The corresponding efficiency (number of emitted photons per electron) was calculated as presented in Figure 3f. The highest efficiency appeared at the most suitable position ( $V_g = 8$  V, equivalent gap for HOMO and LUMO to the Fermi level) of the molecular orbital with the required  $V_w$  ( $\approx 3.5$  V), indicating the best input range for the SM-LED. The maximum efficiency (i.e., the external quantum efficiency,  $\approx 10^{-9}$ ) was not comparable to the macroscopic value ( $\approx 20\%$ ), mainly owing to the large photon loss of the single molecule in the macroscopic

optical measurement path and undesirable blinking. The latter could be attributed to the inherent excitation–emission process, the sojourn into a formed nonemissive triplet state, and the influence of the energy level alignment by the thermal fluctuation. Higher efficiency can be achieved via integrating multiple molecules into the SM-LED by the assistance of “bridge pier” molecules (4-aminobenzoic acid and 4'-amino-biphenyl-4-carboxylic acid, the corresponding schematic was provided in Figure S19 in the Supporting Information). Because of the widening distribution of the lengths, the molecule bridges have higher probability to be integrated into the electrode pairs, which can be further characterized by the super-resolution imaging (Figure 3g). An obvious increase of the efficiency



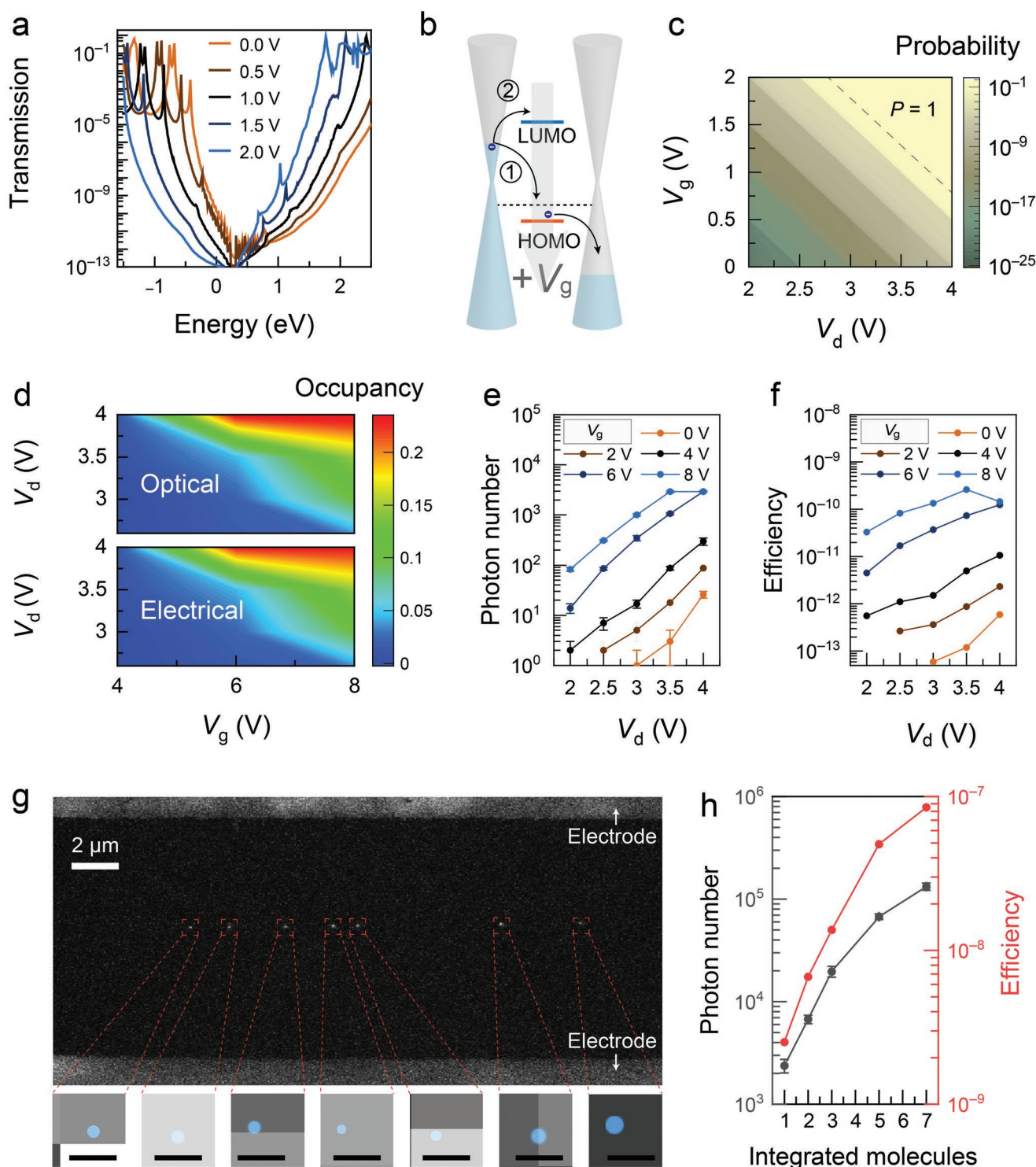


**Figure 3.** Efficiency regulation of an SM-LED. a) Theoretical transmission spectra of the SM-LED under different  $V_g$  (0–2 V). b) Schematic representation of two paths for electron transmission and the regulation of the molecular orbital versus the Fermi level of the electrode. c) Theoretical probability of an SM-LED to emit photons. d) Variations of the occupancy of the bright state with  $V_d$  and  $V_g$ . The results were derived from the optical and electrical signals in Figures S7–S11 (Supporting Information), respectively. e) Variations of the emitted photon numbers with  $V_d$  and  $V_g$ . f) The corresponding efficiency of (e) for one electron to produce a photon with  $V_d$  and  $V_g$ . g) 0.2 mM 4-aminobenzoic acid, 0.2 mM 4'-amino-biphenyl-4-carboxylic acid, and 0.1 mM molecular bridges were added to the graphene electrode pair array to enhance the connection probability. A super-resolution imaging of integrating 7 molecules between one pair of Au electrodes was provided, where the excitation light was 365 nm at  $V_d = 4$  V and  $V_g = 6$  V. The bottom panels show the enlarged images with the scale bar of 100 nm. h) The detected photon numbers and the corresponding calculated efficiency versus integrated molecules at  $V_d = 4$  V and  $V_g = 6$  V.

(to  $\approx 10^{-7}$ , Figure 3h) was found at the integration from 1 to 7 molecules (Figure 3g and Figures S20–S23 (Supporting Information)). This should be attributed to the cooperative effect of multiple molecules, which minimizes individual differences (blinking) at time scales and avoids the resting of radiation at the detection window by asynchronous blinking. The connection of multiple molecules shows the advantage of 2D graphene electrodes, affording the ability to prepare a high-integrated LED.

#### 4. Single-Photon Emission

The energy-resolved single-photon counter was further introduced to the photoelectrical integration system to characterize the EL properties of the SM-LED (Figure S5, Supporting Information). Long-term photon counting is presented in Figure 4a,c ( $V_d = 4$  V and  $V_g = 8$  V), including the corresponding statistical

results on time and energy scales. The thermal fluctuation behavior of the single molecule was represented by nonuniformly distributed photon numbers on the time scale (where the statistical results conform to a Poisson distribution, Figure S24, Supporting Information), which contribute to blinking at the single-molecule site (Videos S1–S3, Supporting Information), the corresponding fluorescent stochastic switching (Figure 2c,g), and STORM imaging (Figure 1b,f). Interestingly, characteristics tending to separate individual photons on the time scale can be obtained at low-level electric inputs ( $V_d = 2$  V and  $V_g = 4$  V) owing to the time resolution being sufficient (Figures S24 and S25, Supporting Information). Moreover, Video S4 (Supporting Information) shows the one-by-one recording of photons in real time. With high electric inputs ( $V_d = 4$  V and  $V_g = 8$  V), the more emitted photons were split into two parts (50/50) by a beam splitter and detected by two single-photon avalanche diodes, respectively. The second-order correlation functions  $g^2(\tau)$  versus different time delays are

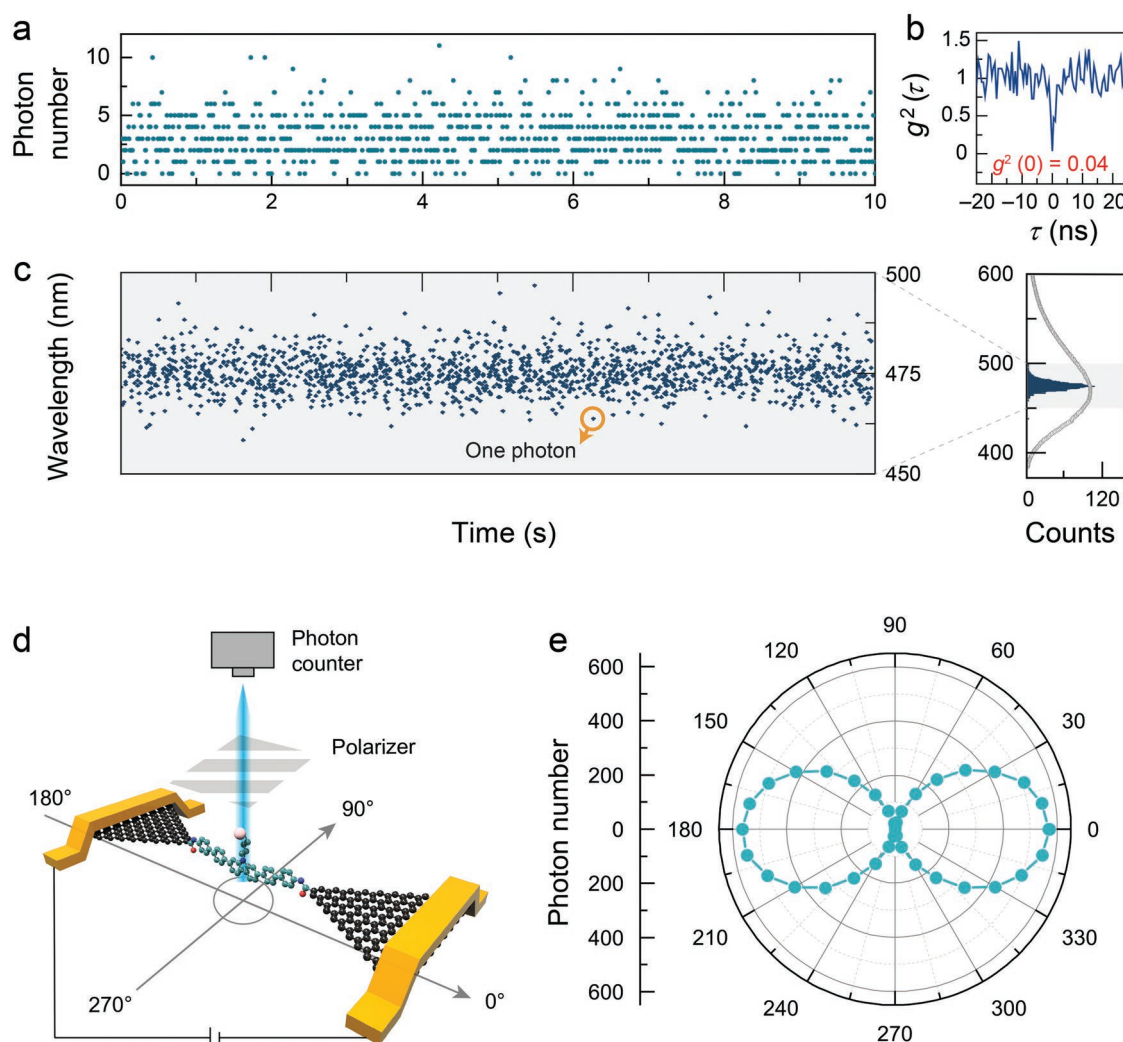


**Figure 4.** Photon emission of an SM-LED. a) Statistical results of (c), the photons emitted from an SM-LED as a function of time. b) Second-order correlation measurement of an SM-LED with electric inputs of  $V_d = 4$  V and  $V_g = 8$  V. c) Counting of emitted photons from the same SM-LED. The statistical results at energy are shown in the right panel, where the gray line represents the macroscopic spectrum.  $V_d = 4$  V and  $V_g = 8$  V. d) Experimental setup to detect the polarization of the emitted photons. e) SM-EL polar diagram at  $V_d = 3$  V and  $V_g = 6$  V.

provided in Figure 4b. The result ( $g^2(0) = 0.04$ ) demonstrates the antibunching effect of the photons at the time scale.<sup>[40]</sup> This is important because the LED prepared by only one molecule is clearly a promising single-photon source that has particular potential applications in quantum computation and communication.<sup>[7]</sup>

## 5. Superior Color Purity

The statistical results show that the emission peak is centered at  $\approx 475$  nm (Figure 4c, right panel), which is consistent with the macroscopic spectrum (gray line), therefore demonstrating that the EL indeed originates from the integrated single molecule. Note that we failed to observe a subtle Stark shift (micro-electron-volt to milli-electron-volt) of the emission peak under the high bias voltage probably because this effect requires micro-electron-volt energy resolution (only milli-electron-volt energy resolution in our current instrument) and is usually measured at low temperature.<sup>[41]</sup> The FWHM is only  $\approx 13$  nm and is narrower than the emission spectrum of the current blue quantum dots and the molecule itself ( $\approx 100$  nm). This indicates superior color purity of the SM-LED, which probably results from the confined freedom of the single molecule between the electrode pairs. The fluorescein molecule with more freedom (introduced by side functionalization) in the junction has an emission spectrum with a FWHM that is comparable to that of the macroscopic spectrum (Figure 5c,d, more details will be provided below), supporting this mechanism.

## 6. Linearly Polarized Light Emission

The fixed molecule in the junction also has fluorescence anisotropy<sup>[42]</sup> (e.g., the polarized LED). Here, the single molecule was integrated in the electrodes and its orientation was determined. A linear polarizer was placed parallel to the chip plane and we defined its orientation along to the electrode pairs as  $0^\circ$ . The emitted light was detected by a photon counter through rotating the linear polarizer (Figure 4d). Periodic variation of the emitted photons ( $N_{\max} = 567 \pm 10$  at  $0^\circ$  and  $180^\circ$ ;  $N_{\min} = 5 \pm 3$  at  $90^\circ$  and  $270^\circ$ ) was observed, which demonstrates a linearly polarized emission (Figure 4e). The polarization  $P \approx 0.98$  can be calculated by  $P = (N_{\max} - N_{\min}) / (N_{\max} + N_{\min})$ . The covalent integration of molecules with fixed orientation provides a new insight into preparing linearly polarized LEDs and also offers more possibility to produce circular polarized light by spin injection.<sup>[43]</sup>

## 7. Color Regulation

In addition to the monochromatic (blue) light emission, the multichromatic SM-LED can be prepared by rational modification of the side group. Similar to current backlit display technology,<sup>[44]</sup> the Förster resonance energy transfer (FRET) strategy can be adopted in the SM-LED through molecular engineering for the multichromatic display.<sup>[45]</sup> The ratio of the emitted light from the donor and acceptor determines the mixed color, which

is affected by the efficiency of FRET ( $E_{\text{FRET}}$ ), quantitatively described by<sup>[46]</sup>

$$E_{\text{FRET}} = \frac{1}{1 + \frac{A \times R^6}{0.529 \times \kappa^2 \times \phi_D \times J(\lambda)}} \quad (1)$$

where  $R$  is the distance between the donor and acceptor,  $\kappa$  is the relative orientation of the dipole between them,  $\phi_D$  is the quantum yield of the donor,  $J(\lambda)$  is the overlap integration of the spectra, and  $A$  is a constant value for a definite system.

The blue-color SM-LED can be used as the donor and the side chain provides an interface to connect the acceptor. Fluorescein is a suitable candidate owing to its large spectral overlap with the molecular bridge (Figure 5f). The connection between them was realized through nucleophilic substitution (Figure S26, Supporting Information). In the current case,  $E_{\text{FRET}}$  can be regulated only by the orientation of the dipole ( $\kappa^2$ ) of the acceptor (because of fixed  $R$ ,  $\phi_D$ , and  $J(\lambda)$  of the donor on the molecular junction). Owing to the presence of PDMS around the molecular junction, the acceptor movement can be restricted by the cross-linking degree of the PDMS (Figure 5a,b). To accurately compare the color regulation, the same modified SM-LED was characterized during the cross-linking of PDMS (time-dependent measurements, Figure 5c,d and Figures S27–S32 (Supporting Information)).

The dipole was effectively restricted after 5 h of PDMS cross-linking and the characteristic EL peak of the molecular bridge (centered at  $\approx 475$  nm) was gradually detected (Figure 5d and Figures S27–S32 (Supporting Information)), implying the energy-preferred conformation with the dipole orthogonal to the molecular bridge. As shown in Figure 5d,e (switching of  $E_{\text{FRET}}$  between 0 and 1), the anticorrelation of the emitting behavior on the time scale further demonstrates the FRET mechanism. The dynamic characterization of the switching between FRET on/off states is presented in Table S1 (Supporting Information), shedding light on the frustrated conformation variations. The results of control experiments based on an SM-LED with the acceptor pyrene (having no obvious spectral overlap) are presented in Figures S33–S35 (Supporting Information), where no emission of pyrene was observed, again supporting the FRET mechanism.

Furthermore, the mixed color can be located on the Commission International de l'Eclairage (CIE) chromaticity diagram (Figure 5g). The inset shows the occupancy of the donor and acceptor emissions during the different cross-linking stages. With an increase in the ratio of the donor emission, the mixed color shifts from (0.30, 0.68) to (0.23, 0.43) on the CIE chromaticity diagram, implying that precise manipulation of the acceptor conformation in the future can realize color tunability for a single SM-LED, which is an alternative strategy for improving integration.

In addition, the replaceability of the acceptor provides another ability to regulate the emitted color. For example, a resorufin-derived SM-LED shows a shift in emission to the red-color range (Figures S36–S39, Supporting Information). In summary, colority of the SM-LED can be varied by modifying the donor (i.e., the molecular bridge in obtaining higher color purity) and the acceptor (in obtaining lower color purity) or



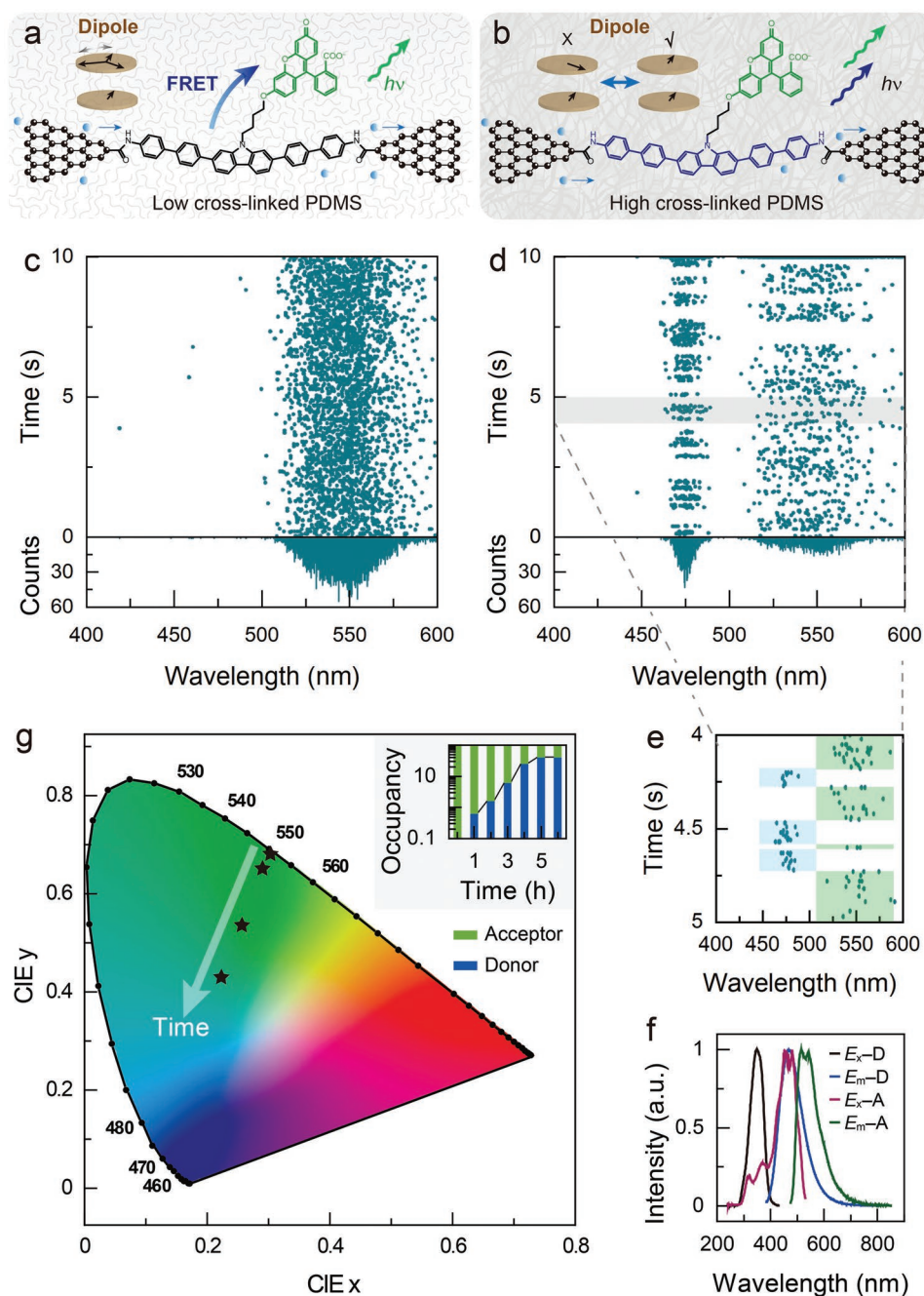


**Figure 5.** Color regulation of an SM-LED. a) Schematic representation of an SM-LED in the low cross-linked PDMS. The fluorescein acceptor has the freedom to undergo conformational changes and receives the energy transferred from the molecular bridge. b) Schematic representation of an SM-LED in the high cross-linked PDMS. The conformation of fluorescein was restricted and has a slow conversion between the orthogonal (inhibited for FRET) and nonorthogonal dipole states at room temperature. c) Recorded photons of an SM-LED in the low cross-linked PDMS.  $V_d = 4$  V and  $V_g = 8$  V. d) Recorded photons of the same SM-LED in the high cross-linked PDMS.  $V_d = 4$  V and  $V_g = 8$  V. e) Enlargement of the panel in (d), clearly showing the photon emission of the donor (the molecular bridge) without FRET, and the disappearance of donor emission and simultaneous appearance of acceptor emission (fluorescein) after FRET. f) Macroscopic excitation ( $E_x$ ) and emission ( $E_m$ ) spectra of the molecular bridge (the donor: D) and fluorescein (the acceptor: A). Both of them are  $10^{-5}$  mol  $L^{-1}$  in ethanol solution. g) Located emitted color in the CIE chromaticity diagram with PDMS at the different cross-linking times. Inset: occupancy of the donor and acceptor emission during PDMS cross-linking.

regulating  $E_{FRET}$  (through controlling the molecular conformation) to meet the requirements of real display and illumination. We believe that a full range of pure color can be achieved for the SM-LED by taking advantage of flexible organic synthesis and conformation regulation.

## 8. Conclusion

We have created a class of covalently bonded stable SM-LEDs, which show color tunability with high purity, linear polarization, precise control of the photon number (brightness) and efficiency,



excellent resolution (<200 nm per pixel), single-photon emission, and reproducibility. We thus open up new opportunities for developing the next generation of optoelectronics, high-resolution displays, and quantum communication. Along the lines of evolutionary organic LEDs and QD-LEDs, further optimization of the SM-LED requires thorough investigations in the fields of interface engineering (relating to the mechanism of electron transmission), molecular engineering (relating to the inherent quantum yield), and device architecture (relating to the total efficiency). In addition, the SM-LED brings the advantages of precise regulation through external stimuli, offering new insights into the development of multifunctional devices involving the modulation of optical, electrical, and magnetic signals. Viewed from another perspective, the accurate detection of the photon would inspire multimodal measurements of molecular behaviors. Specifically, the complete understanding of the intrinsic photophysics necessitates the synchronous characterization of optical and electrical properties with high resolution. Upon further combination with ultrafast or ultracold techniques, this strategy shows great promise for the precise detection of single molecule/electron/photon/quantum states in chemical and biological processes, which invites intense studies.

## Supporting Information

Supporting Information is available from the Wiley Online Library or from the author.

## Acknowledgements

C.Y. and Y.G. contributed equally to this work. The authors thank Yunfeng Xiao, Wenjing Liu, and Ang Gao for their technical support of the second-order correlation measurements. The authors acknowledge primary financial supports from the National Key R&D Program of China (Grant Nos. 2021YFA1200101, 2017YFA0204901, and 2022YFE0128700), the National Natural Science Foundation of China (Grant Nos. 22150013, 21727806, and 21933001), the Tencent Foundation through the XPLOER PRIZE, the Natural Science Foundation of Beijing (Grant No. 2222009), and the “Frontiers Science Center for New Organic Matter” at Nankai University (Grant No. 63181206).

## Conflict of Interest

The authors declare no conflict of interest.

## Data Availability Statement

The data that support the findings of this study are available from the corresponding author upon reasonable request.

## Keywords

electroluminescence, Förster resonance energy transfer, single-molecule light-emitting diodes, single-photon emission

Received: October 22, 2022

Revised: January 1, 2023

Published online:

- [1] H. Cho, S.-H. Jeong, M.-H. Park, Y.-H. Kim, C. Wolf, C.-L. Lee, J. H. Heo, A. Sadhanala, N. Myoung, S. Yoo, S. H. Im, R. H. Friend, T.-W. Lee, *Science* **2015**, 350, 1222.
- [2] F. Yuan, Y.-K. Wang, G. Sharma, Y. Dong, X. Zheng, P. Li, A. Johnston, G. Bappi, J. Z. Fan, H. Kung, B. Chen, M. I. Saidaminov, K. Singh, O. Voznyy, O. M. Bakr, Z.-H. Lu, E. H. Sargent, *Nat. Photonics* **2020**, 14, 171.
- [3] L. Qian, Y. Zheng, J. Xue, P. H. Holloway, *Nat. Photonics* **2011**, 5, 543.
- [4] C. Pan, L. Dong, G. Zhu, S. Niu, R. Yu, Q. Yang, Y. Liu, Z. L. Wang, *Nat. Photonics* **2013**, 7, 752.
- [5] Y. Xiao, W. Xiao, D. Wu, L. Guan, M. Luo, L.-D. Sun, *Adv. Funct. Mater.* **2022**, 32, 2109618.
- [6] X. Dai, Y. Deng, X. Peng, Y. Jin, *Adv. Mater.* **2017**, 29, 1607022.
- [7] H.-S. Zhong, H. Wang, Y.-H. Deng, M.-C. Chen, L.-C. Peng, Y.-H. Luo, J. Qin, D. Wu, X. Ding, Y. Hu, P. Hu, X.-Y. Yang, W.-J. Zhang, H. Li, Y. Li, X. Jiang, L. Gan, G. Yang, L. You, Z. Wang, L. Li, N.-L. Liu, C.-Y. Lu, J.-W. Pan, *Science* **2020**, 370, 1460.
- [8] A. Polman, M. Knight, E. C. Garnett, B. Ehrler, W. C. Sinke, *Science* **2016**, 352, aad4424. doi:10.1126/science.aad4424.
- [9] Y. Shirasaki, G. J. Supran, M. G. Bawendi, V. Bulović, *Nat. Photonics* **2013**, 7, 13.
- [10] C. Edwards, *Commun. ACM* **2021**, 64, 12.
- [11] D. Xiang, X. Wang, C. Jia, T. Lee, X. Guo, *Chem. Rev.* **2016**, 116, 4318.
- [12] N. Xin, J. X. Guan, C. G. Zhou, X. J. N. Chen, C. H. Gu, Y. Li, M. A. Ratner, A. Nitzan, J. F. Stoddart, X. F. Guo, *Nat. Rev. Phys.* **2019**, 1, 211.
- [13] A. Aviram, M. A. Ratner, *Chem. Phys. Lett.* **1974**, 29, 277.
- [14] L. Meng, N. Xin, C. Hu, H. A. Sabea, M. Zhang, H. Jiang, Y. Ji, C. Jia, Z. Yan, Q. Zhang, L. Gu, X. He, P. Selvanathan, L. Norel, S. Rigaut, H. Guo, S. Meng, X. Guo, *Nat. Commun.* **2022**, 13, 1410.
- [15] H. Song, Y. Kim, Y. H. Jang, H. Jeong, M. A. Reed, T. Lee, *Nature* **2009**, 462, 1039.
- [16] N. Xin, C. Hu, H. Al Sabea, M. Zhang, C. Zhou, L. Meng, C. Jia, Y. Gong, Y. Li, G. Ke, X. He, P. Selvanathan, L. Norel, M. A. Ratner, Z. Liu, S. Xiao, S. Rigaut, H. Guo, X. Guo, *J. Am. Chem. Soc.* **2021**, 143, 20811.
- [17] B. Capozzi, J. L. Xia, O. Adak, E. J. Dell, Z. F. Liu, J. C. Taylor, J. B. Neaton, L. M. Campos, L. Venkataraman, *Nat. Nanotechnol.* **2015**, 10, 522.
- [18] C. Jia, A. Migliore, N. Xin, S. Huang, J. Wang, Q. Yang, S. Wang, H. Chen, D. Wang, B. Feng, Z. Liu, G. Zhang, D.-H. Qu, H. Tian, M. A. Ratner, H. Q. Xu, A. Nitzan, X. Guo, *Science* **2016**, 352, 1443.
- [19] L. N. Meng, N. Xin, C. Hu, J. Y. Wang, B. Gui, J. J. Shi, C. Wang, C. Shen, G. Y. Zhang, H. Guo, S. Meng, X. F. Guo, *Nat. Commun.* **2019**, 10, 1450.
- [20] K. K. Zhang, C. Wang, M. H. Zhang, Z. B. Bai, F. F. Xie, Y. Z. Tan, Y. L. Guo, K. J. Hu, L. Cao, S. Zhang, X. C. Tu, D. F. Pan, L. Kang, J. Chen, P. H. Wu, X. F. Wang, J. L. Wang, J. M. Liu, Y. Song, G. H. Wang, F. Q. Song, W. Ji, S. Y. Xie, S. F. Shi, M. A. Reed, B. G. Wang, *Nat. Nanotechnol.* **2020**, 15, 1019.
- [21] C. C. Jia, X. F. Guo, *Chem. Soc. Rev.* **2013**, 42, 5642.
- [22] J. Kern, R. Kullock, J. Prangsma, M. Emmerling, M. Kamp, B. Hecht, *Nat. Photonics* **2015**, 9, 582.
- [23] X. H. Qiu, G. V. Nazin, W. Ho, *Science* **2003**, 299, 542.
- [24] C. W. Marquardt, S. Grunder, A. Błaszczyk, S. Dehm, F. Henrich, H. v. Löhneysen, M. Mayor, R. Krupke, *Nat. Nanotechnol.* **2010**, 5, 863.
- [25] G. Reecht, F. Scheurer, V. Speisser, Y. J. Dappe, F. Mathevet, G. Schull, *Phys. Rev. Lett.* **2014**, 112, 047403.
- [26] L. Zhang, Y.-J. Yu, L.-G. Chen, Y. Luo, B. Yang, F.-F. Kong, G. Chen, Y. Zhang, Q. Zhang, Y. Luo, J.-L. Yang, Z.-C. Dong, J. G. Hou, *Nat. Commun.* **2017**, 8, 580.
- [27] W. Du, T. Wang, H.-S. Chu, L. Wu, R. Liu, S. Sun, W. K. Phua, L. Wang, N. Tomczak, C. A. Nijhuis, *Nat. Photonics* **2016**, 10, 274.

- [28] U. M. Tefashe, Q. V. Nguyen, F. Lafolet, J.-C. Lacroix, R. L. McCreery, *J. Am. Chem. Soc.* **2017**, *139*, 7436.
- [29] M. C. Chong, L. Sosa-Vargas, H. Bulou, A. Boeglin, F. Scheurer, F. Mathevet, G. Schull, *Nano Lett.* **2016**, *16*, 6480.
- [30] M. C. Chong, N. Afshar-Imani, F. Scheurer, C. Cardoso, A. Ferretti, D. Prezzi, G. Schull, *Nano Lett.* **2018**, *18*, 175.
- [31] M. C. Chong, G. Reecht, H. Bulou, A. Boeglin, F. Scheurer, F. Mathevet, G. Schull, *Phys. Rev. Lett.* **2016**, *116*, 036802.
- [32] Y. Li, C. Yang, X. F. Guo, *Acc. Chem. Res.* **2020**, *53*, 159.
- [33] Q. Xu, G. Scuri, C. Mathewson, P. Kim, C. Nuckolls, D. Bouilly, *Nano Lett.* **2017**, *17*, 5335.
- [34] M. J. Rust, M. Bates, X. Zhuang, *Nat. Methods* **2006**, *3*, 793.
- [35] L. Gaudreau, K. J. Tielrooij, G. E. D. K. Prawiroatmodjo, J. Osmond, F. J. G. de Abajo, F. H. L. Koppens, *Nano Lett.* **2013**, *13*, 2030.
- [36] A. Brenneis, L. Gaudreau, M. Seifert, H. Karl, M. S. Brandt, H. Huebl, J. A. Garrido, F. H. L. Koppens, A. W. Holleitner, *Nat. Nanotechnol.* **2015**, *10*, 135.
- [37] H. Ishii, K. Sugiyama, E. Ito, K. Seki, *Adv. Mater.* **1999**, *11*, 605.
- [38] A. Rajagopal, Z. Yang, S. B. Jo, I. L. Braly, P.-W. Liang, H. W. Hillhouse, A. K. Y. Jen, *Adv. Mater.* **2017**, *29*, 1702140.
- [39] Z. C. Dong, X. L. Zhang, H. Y. Gao, Y. Luo, C. Zhang, L. G. Chen, R. Zhang, X. Tao, Y. Zhang, J. L. Yang, J. G. Hou, *Nat. Photonics* **2010**, *4*, 50.
- [40] R. H. Brown, R. Q. Twiss, *Nature* **1956**, *177*, 27.
- [41] H. Imada, M. Imai-Imada, K. Miwa, H. Yamane, T. Iwasa, Y. Tanaka, N. Toriumi, K. Kimura, N. Yokoshi, A. Muranaka, M. Uchiyama, T. Taketsugu, Y. K. Kato, H. Ishihara, Y. Kim, *Science* **2021**, *373*, 95.
- [42] D. M. Jameson, J. A. Ross, *Chem. Rev.* **2010**, *110*, 2685.
- [43] Y. H. Kim, Y. X. Zhai, H. P. Lu, X. Pan, C. X. Xiao, E. A. Gaulding, S. P. Harvey, J. J. Berry, Z. V. Vardeny, J. M. Luther, M. C. Beard, *Science* **2021**, *371*, 1129.
- [44] E. Jang, S. Jun, H. Jang, J. Llim, B. Kim, Y. Kim, *Adv. Mater.* **2010**, *22*, 3076.
- [45] R. P. Puchert, F. Steiner, G. Plechinger, F. J. Hofmann, I. Caspers, J. Kirschner, P. Nagler, A. Chernikov, C. Schuller, T. Korn, J. Vogelsang, S. Bange, J. M. Lupton, *Nat. Nanotechnol.* **2017**, *12*, 637.
- [46] A. Iqbal, S. Arslan, B. Okumus, T. J. Wilson, G. Giraud, D. G. Norman, T. Ha, D. M. J. Lilley, *Proc. Natl. Acad. Sci. USA* **2008**, *105*, 11176.